

Lyapunov Spectrum Scaling for Classical Many-Body Dynamics Close to Integrability

Merab Malishava^{*} and Sergej Flach[†]*Center for Theoretical Physics of Complex Systems, Institute for Basic Science (IBS), Daejeon 34126, Korea and Basic Science Program, Korea University of Science and Technology (UST), Daejeon 34113, Korea* (Received 16 August 2021; revised 2 December 2021; accepted 8 March 2022; published 31 March 2022)

We propose a novel framework to characterize the thermalization of many-body dynamical systems close to integrable limits using the scaling properties of the full Lyapunov spectrum. We use a classical unitary map model to investigate macroscopic weakly nonintegrable dynamics beyond the limits set by the KAM regime. We perform our analysis in two fundamentally distinct long-range and short-range integrable limits which stem from the type of nonintegrable perturbations. Long-range limits result in a single parameter scaling of the Lyapunov spectrum, with the inverse largest Lyapunov exponent being the only diverging control parameter and the rescaled spectrum approaching an analytical function. Short-range limits result in a dramatic slowing down of thermalization which manifests through the rescaled Lyapunov spectrum approaching a non-analytic function. An additional diverging length scale controls the exponential suppression of all Lyapunov exponents relative to the largest one.

DOI: 10.1103/PhysRevLett.128.134102

Thermalization is a universal property of the long-time dynamics of generic nonintegrable many-body systems. Thermal equilibrium is characterized by stationary distributions and assumes ergodicity and mixing in the phase space [1]. The thermalization dynamics will in general slow down close to integrability, and may even cease to be observed [2–8], which was also noted in earlier studies of dynamical systems [9–12]. The theory of weak nonintegrable perturbations for finite Hamiltonian systems $H = H_0 + \varepsilon H_1$ was pioneered by Kolmogorov in 1954 [13] and later by Arnold [14] and Moser [15], here H_0 and H_1 refers to integrable and nonintegrable parts of the Hamiltonian, respectively. The corresponding KAM theory demonstrates the violation of the ergodic hypothesis for sufficiently weak perturbations due to the emergence of a mixed phase space with a finite fraction of points belonging to regular trajectories on tori. At a critical strength of the nonintegrable perturbation ε , all tori disappear, and the dynamics become fully chaotic allowing for thermalization. But what exactly is meant by “sufficiently weak” and “critical strength”? As it turns out the magnitude of the critical perturbation ε decays rapidly with the growth of the number of degrees of freedom. Namely, $\varepsilon \leq aN^{-b}$ with $b = 160$ has been shown as an upper bound for applicability of KAM theory in lattice systems with short-range interactions (for example, an array of Josephson junctions) [16]. This result suggests that it is practically impossible to witness quasiperiodic motion suggested by KAM in macroscopically large systems close to integrability. What is then the expected behavior of systems with a large number of degrees of freedom in proximity to an integrable limit? How does one characterize it? Does it have universality classes? Is there a KAM-like regime for macroscopic

models? If not, what lies beyond the KAM horizon spanned by finite systems?

To quantify the thermalization of a system one typically chooses a specific set of observables and studies

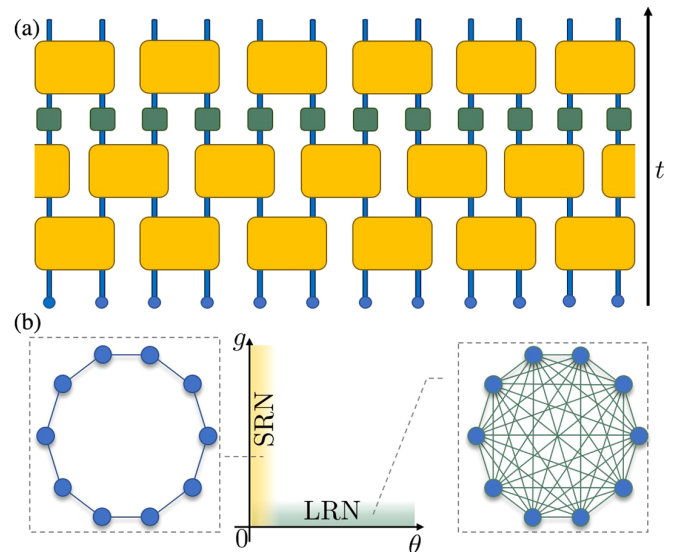


FIG. 1. (a) A schematic representation of the unitary circuits map. Large yellow blocks indicate \hat{C} unitary matrices parametrized by the angle θ . Small green blocks indicate local nonlinearity generating map \hat{G} parametrized by the nonlinearity strength g . The black arrow on the right indicates the time flow. (b) Control parameter space $\{\theta, g\}$ with the highlighted area corresponding to the induced networks. Integrable limits are reached for $g = 0$ (linear evolution of extended normal modes) or $\theta = 0$ (decoupled nonlinear map). Small nonzero g values induce LRNs, small nonzero θ values induce SRNs. The network images indicate actions (filled circles) and couplings induced by the nonintegrable perturbation (straight lines). Left image, SRN; right image, LRN.

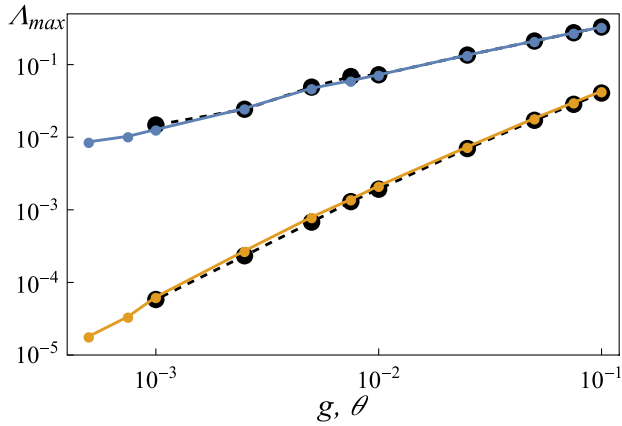


FIG. 2. The largest Lyapunov exponents Λ_{\max} in SRN (blue small circles, top) and LRN (orange small circles, bottom) regime versus the corresponding deviation from integrable limit g, θ . Solid lines connect the data points and guide the eye. For the SRN case, the parameter nonlinearity is fixed $g = 1.0$, while for the LRN case the angle θ is fixed at 0.33π . For both cases system size $N = 200$. The large black circles connected by dashed lines correspond to data for system size $N = 100$.

equipartition and ergodicity for those specific observables. In their pioneering work Fermi, Pasta, Ulam, and Tsingou attempted to showcase equipartition using the normal modes of a linear chain as their choice of observables for a weakly nonlinear chain [17]. In the absence of nonlinearity, the normal modes are “frozen,” i.e., they become the *actions* of the integrable system.

Recent studies attempted to broaden the ergodicity analysis by computing convergence of finite-time average distributions of observables to their phase space averages. They revealed that most physical systems belong to two distinct classes when it comes to thermalization in proximity to integrable limits [18–20]. Systems with weak nonlinear perturbations such as FPUT chains, Josephson junction networks in the limit of small energy density, discrete nonlinear Schrödinger equations all belong to the class of *long range networks* (LRN). On the other hand, a broad range of lattice systems allowing for proximity to an integrable limit of vanishing lattice coupling belongs to a class of *short range networks* (SRN). Examples of SRN include coupled anharmonic oscillator chains in the limit of weak coupling [18], Josephson junction chains in the limit of weak Josephson coupling [19], etc.

There are serious limitations of studying thermalization through observable dynamics. The choice of observables is ambiguous [21,22], and even for integrable systems specifically chosen observables show ergodic thermal-like behavior [23]. Observable dynamics address ergodicity, but not mixing. However, nonintegrable dynamics are necessarily mixing, show typically exponential decay of correlations with a macroscopic set of correlation times.

In this Letter, we overcome the above limitations by computing the entire Lyapunov spectrum [24]. Lyapunov

spectra were previously used for diagnosing phase transitions [25] and energy localization [26]. Here we show that the scaling properties of the Lyapunov spectrum offer a conceptual novel way for the description of weakly non-integrable dynamics in a generic model setup. We consider a macroscopically large system beyond the limits set by KAM and characterize thermalization in both SRN and LRN regimes, thus drawing a very general picture that encapsulates a great number of physically realizable scenarios and is directly applicable to most weakly non-integrable classical systems.

Resolving the entire Lyapunov spectrum for a large system is a numerically challenging task. It relies on the simultaneous evolution of a large number of trajectories, [27]. The proximity to integrable limits makes this task even harder due to an increase of the thermalization times. In view of these challenges, we need models which possess all physically relevant features to achieve thermalization and are extremely efficient for the numerical evolution—unitary maps. The fast, exact, error-free discrete-time evolution is a key feature of unitary maps which makes them advantageous for heavy numerical tasks. These properties were on display in recent studies, where discrete unitary maps were used to achieve record-breaking evolution times for nonlinear wave-packet spreading tasks [28], Anderson localization [29,30], and soliton dynamics [31].

Model.—We use classical unitary circuit maps. We define a 1D lattice of size N with one complex component ψ_n per site n . The classical dynamics evolves the vector $\vec{\Psi} = \{\psi_n\}$ in a corresponding phase space of dimension $2N$ on a deterministic trajectory specified by an initial condition. The evolution is performed by subsequent applications of the map:

$$\hat{U} = \sum_{n \in \mathbb{Z}} \hat{G}_n \sum_{n \in 2\mathbb{Z}+1} \hat{C}_{n,n+1} \sum_{n \in 2\mathbb{Z}} \hat{C}_{n,n+1}. \quad (1)$$

The unitary matrices $\hat{C}_{n,n+1}$ are parametrized by the rotation angle θ and act as hoppings on pairs of neighboring sites:

$$\hat{C}_{n,n+1} \begin{pmatrix} \psi_n(t) \\ \psi_{n+1}(t) \end{pmatrix} = \begin{pmatrix} \cos \theta & \sin \theta \\ -\sin \theta & \cos \theta \end{pmatrix} \begin{pmatrix} \psi_n(t) \\ \psi_{n+1}(t) \end{pmatrix}, \quad (2)$$

and the local map \hat{G}_n induces nonlinearity:

$$\hat{G}_n \psi_n = e^{i g |\psi_n|^2} \psi_n. \quad (3)$$

The classical unitary circuit dynamics is schematically represented in Fig. 1.

The evolution given by unitary matrix maps may be viewed as a generalization of canonical transformations to complex phase-space coordinates. The map dynamics of classical unitary circuits is mixing and therefore ergodic. During the evolution the norm of the state vector $\vec{\Psi}(t)$ is conserved, which leads to the Gibbs distributed absolute

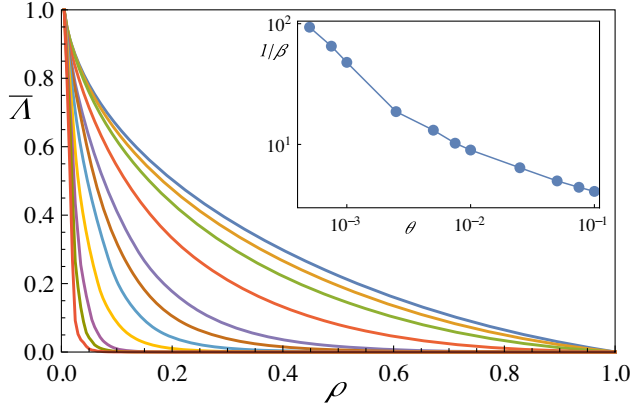


FIG. 3. Renormalized Lyapunov spectrum $\{\bar{\Lambda}\}$ against the rescaled index ρ for SRN in proximity to the integrable limit. The nonlinearity strength is fixed at $g = 1.0$. Angle θ varies from 10^{-1} (blue, top) to 5×10^{-4} (red, bottom). The inset shows the coefficient $1/\beta$ of the exponential decay (see also Fig. 4) of the curves as a function of θ . System size $N = 200$.

values of local components $|\psi_n|^2$. This is analogous to the energy conserving Hamiltonian dynamics with Gibbs distributed local energies. The map possesses two distinct LRN and SRN integrable limits. We checked that the thermalization properties of observables in unitary circuits are in line with previous observations for Hamiltonian systems [18,19].

SRN integrable limit.—We consider the limiting case $\theta = 0$ with a fixed nonzero value of nonlinearity strength g . In this setup the matrices $\hat{C}_{n,n+1}$ become unity, thus decoupling the sites. The unitary evolution applies a nonlinear norm dependent phase shift at each site:

$$\hat{U}_{\text{int}}^{\text{SRN}} \vec{\Psi} = \sum_{n \in \mathbb{Z}} e^{ig|\psi_n|^2} \psi_n. \quad (4)$$

The system turns integrable with the norm at each site $|\psi_n|^2$ being a constant of motion. By introducing a weak deviation from the limit $0 < \theta \ll 1$ one induces a network with next-to-nearest-neighbor hopping—an SRN (see Supplemental Material for more details [32]). We schematically represent the parameter space and corresponding network in Fig. 1(b).

LRN integrable limit.—Vanishing nonlinearity strength $g = 0$ results in a linear evolution with corresponding eigenvalue problem $e^{i\omega} \vec{\Psi}(t) = \hat{U}_{\text{int}}^{\text{LRN}} \vec{\Psi}(t)$ (see details in Supplemental Material [32]). The evolution corresponding to this integrable limit is given by

$$\hat{U}_{\text{int}}^{\text{LRN}} \vec{\Psi} = \sum_k \hat{u}_k \vec{\psi}_k, \quad (5)$$

where $\vec{\psi}_k$ are the normal modes of the system and u_k is the evolution map in reciprocal space corresponding to the wave number k . In this limit the absolute values of the

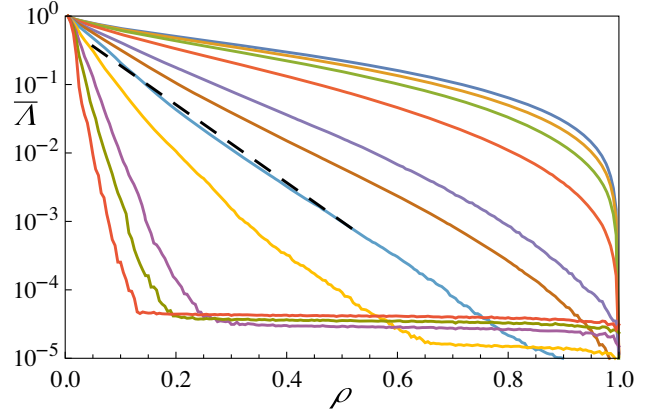


FIG. 4. Renormalized Lyapunov spectrum $\{\bar{\Lambda}\}$ against the rescaled index ρ for SRN in log scale (corresponding to the parameters and data of Fig. 3). The dashed line is to guide the eye for the fit of exponential decay.

normal mode amplitudes $|c_k| = |\vec{\psi}_k^\dagger \cdot \vec{\Psi}(t)|$ are the constants of motion. The deviation from this limit $g \neq 0$ induces an all-to-all coupling among the normal modes of the system which respects translational invariance through selection rules [32]. This by definition constitutes an LRN. The green region in the control parameter space in Fig. 1(b) corresponds to that LRN with the schematic representation of the network sketched right to it.

We compute the Lyapunov spectrum of unitary circuits in proximity to integrable limits in order to resolve the entire set of characteristic timescales. We follow the evolution of a set of orthogonal tangent vectors $\{\vec{w}_i\}$ in the $2N$ dimensional phase space and compute the increment $\gamma_i(t) = |\vec{w}_i(t)|$. Details on the approach can be found in Sec. V of the Supplemental Material [32]. For each vector we compute the transient value $X_i(t) = 1/t \sum_{\tau}^t \log \gamma(\tau)$ which in the infinite time limit turns into the Lyapunov characteristic exponent (LCE) $\Lambda_i = \lim_{t \rightarrow \infty} X_i(t)$. The numerically computed LCEs are the values of $X(t)$ extracted at the last step of the dynamics. The LCEs are ordered from largest to smallest value upon incrementing the index i . Because of the symplectic nature of the map the spectrum is symmetric with LCEs coming in pairs $\Lambda_i = -\Lambda_{2N-i+1}$. Norm conservation ensures two vanishing LCEs $\Lambda_N = \Lambda_{N+1} = 0$ [33]. According to the numerical setup, however, it is impossible to achieve exact $\Lambda_i = 0$ values, with bounds on the smallest computed Lyapunov exponents $\Lambda_{\min} \sim 1/t$.

The evolution of the phase space vector $\vec{\Psi}$ is obtained from subsequent applications of the map \hat{U} . We use periodic boundary conditions $\psi_{N+1} = \psi_1$. The initial conditions for the amplitudes of the local complex components are drawn from an exponential distribution $p(x) = e^{-x}$, while their phases were generated as uncorrelated and random numbers chosen uniformly from the interval $[0, 2\pi]$. The state vector is then uniformly rescaled

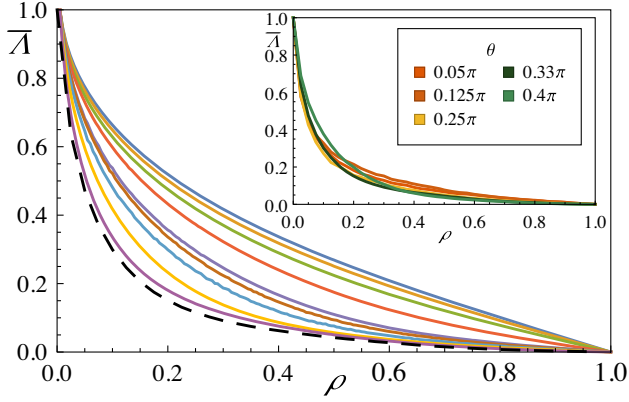


FIG. 5. Renormalized Lyapunov spectrum $\{\bar{\Lambda}\}$ against the rescaled index ρ for LRN in proximity to the integrable limit. The angle $\theta = 0.33\pi$ is fixed. The deviation from the integrable limit g varies from 10^{-1} (blue) to 10^{-3} (purple). The dashed line is to show the asymptotic curve as $g \rightarrow 0$. In the inset we showcase the asymptotic curve as parameter θ is varied. For all cases system size $N = 200$.

such that the norm density $(1/N) \sum |\psi_n|^2 = 1$. The largest integration time varied between $t_{\max} = 10^8$ and $t_{\max} = 10^9$. We have performed computations for a set of initial conditions to ensure the independence of results on the choice of initial state. Unless stated otherwise the system size is set to $N = 200$.

First, we show the dependence of the largest Lyapunov exponent Λ_{\max} on the distance g or θ to the integrable limit in Fig. 2 for both networks. Both curves show a dependence which might resemble a power law $\Lambda_{\max} \sim g^\nu$ and $\Lambda_{\max} \sim \theta^\mu$ with $\nu \approx 1/2$ and $\mu \approx 3/2$. Remarkably the SRN case shows a much slower diminishing of Λ_{\max} upon approaching the integrable limit as compared to the LRN. This is similar to the study of a Hamiltonian system dynamics [18,34,35]. Our data in Fig. 2 are obtained for two different system sizes $N = 100, 200$ and show very good agreement, therefore we can exclude finite-size corrections. We now proceed to the analysis of the entire Lyapunov spectrum. In Figs. 3 and 5 we show the renormalized Lyapunov spectrum $\bar{\Lambda}_i = \Lambda_i/\Lambda_{\max}$ for SRN and LRN respectively. The index of Lyapunov exponents is rescaled $\rho = i/N$ so that all positive LCEs $\bar{\Lambda}(\rho)$ correspond to $\rho \in [0, 1]$. We notice a dramatic qualitative difference between the two regimes. For the LRN case the renormalized Lyapunov spectrum $\bar{\Lambda}(\rho)$ converges to a limiting smooth curve for $g \rightarrow 0$. For the SRN instead that curve vanishes in an exponential way. We will explain these observations in detail below.

For the SRN an increasing number of Lyapunov exponents seems to be vanishing upon approaching the integrable limit as seen in Fig. 3. We replot the same spectrum in log scale in Fig. 4 and notice an exponential decay of the renormalized spectrum:

$$\Lambda_\rho^{\text{SRN}} = \Lambda_{\max} e^{-\rho/\beta}. \quad (6)$$

We fit the exponential decay and plot the exponent $1/\beta$ versus θ in the inset in Fig. 3. We observe that the exponent is rapidly diverging upon approaching the integrable limit such that $\beta(\theta \rightarrow 0) \rightarrow 0$. The entire Lyapunov spectrum of the SRN is therefore characterized by two scaling parameters—the largest Lyapunov exponent Λ_{\max} which is an inverse timescale, and the parameter β which is an inverse length scale. This result explains and agrees with previous studies on dynamical glass in Hamiltonian systems [18,19] where the largest Lyapunov exponent stems from local resonances with rapidly increasing distance between them upon approaching the integrable limit. Our results show that the Lyapunov spectrum contains the quantitative scaling parameters of that dynamical glass theory.

In contrast, the LRN spectrum is characterized by single parameter scaling. The renormalized Lyapunov spectrum approaches a smooth limiting curve $\bar{\Lambda}(\rho)$ as seen in Fig. 5. We compute the limiting curves by a linear fit of $\bar{\Lambda}_\rho(g)$ at each value of ρ_j . Thus in the LRN regime, the final form of the spectrum is given by

$$\Lambda_\rho^{\text{LRN}} = \Lambda_{\max} f(\rho, \theta). \quad (7)$$

The limiting curves for different values of θ are plotted in the inset of Fig. 5 and show little if any variation. It appears that the limiting curve $f(\rho)$ is universal for all LRN parameter choices.

To further characterize the chaotic dynamics and showcase the difference between SR and LR networks we compute the Kolmogorov-Sinai entropy $K_{\text{KS}} = \int_0^1 \bar{\Lambda}_\rho d\rho$. In the SRN case, from Eq. (6) follows

$$K_{\text{KS}}^{\text{SRN}} = \Lambda_{\max} \beta (1 - e^{-1/\beta}). \quad (8)$$

Therefore, the renormalized Kolmogorov-Sinai entropy $k_{\text{KS}} = K_{\text{KS}}/\Lambda_{\max}$ will tend to zero in the integrable limit $k_{\text{KS}} \approx \beta$.

In the LRN regime the integral over the asymptotic function $f(\rho, \theta)$ [see Eq. (7)] will lead to finite values of the renormalized KS entropy $k_{\text{KS}} = \int_0^1 f(\rho) d\rho > 0$ at the very integrable limit.

To conclude, we identified the Lyapunov spectrum as a universal characteristic descriptor of the complex phase space dynamics of a macroscopic system in proximity to an integrable limit. The limit is characterized by a macroscopic number of conserved actions. We identify two classes of nonintegrable perturbation networks—short and long-range ones. Long-range networks are characterized by a single parameter scaling of the Lyapunov spectrum—knowing the largest Lyapunov exponent allows to reconstruct the entire spectrum. Consequently, all Lyapunov exponents scale as the largest one upon approaching the integrable limit. Typical long-range

networks are realized with translationally invariant lattice systems in the limit of weak nonlinearity. In that case, the actions correspond to normal modes extended over the entire real space. Nonintegrable perturbations will typically couple them all. On the other side, short-range networks are characterized by a two-parameter scaling. In addition to the largest Lyapunov exponent, a diverging length scale results in a suppression of the renormalized Lyapunov spectrum upon approaching the integrable limit. Typical short-range networks are realized with lattice systems and local (short-range) nonlinearities in the limit of weak coupling. Our findings call for a thorough analysis of other potential network range classes. In particular the cases with disorder, exponentially or polynomially decaying long-range couplings in combination with multiple spatial dimensions may result in new classes of weakly nonintegrable dynamics, which are not covered in this work and could be a promising direction of future research. In particular, quantizing the classical dynamics could lead to many-body localization in the case of short-range networks, as opposed to long-range networks.

This work was supported by the Institute for Basic Science (Project No. IBS-R024-D1).

*Corresponding author.

merabmalishava@gmail.com

†Corresponding author.

sergejflach@googlemail.com

- [1] K. Huang, *Statistical Mechanics*, 2nd ed. (John Wiley & Sons, New York, 1987).
- [2] C. Gogolin, M. P. Müller, and J. Eisert, *Phys. Rev. Lett.* **106**, 040401 (2011).
- [3] M. Rigol, *Phys. Rev. Lett.* **103**, 100403 (2009).
- [4] D. K. Campbell, P. Rosenau, and G. M. Zaslavsky, *Chaos* **15**, 015101 (2005).
- [5] B. Gaveau and L. S. Schulman, *Eur. Phys. J. Special Topics* **224**, 891 (2015).
- [6] J.-P. Bouchaud, *J. Phys. I (France)* **2**, 1705 (1992).
- [7] G. Bel and E. Barkai, *Europhys. Lett.* **74**, 15 (2006).
- [8] G. Bel and E. Barkai, *Phys. Rev. Lett.* **94**, 240602 (2005).
- [9] J. Ford, *Phys. Rep.* **213**, 271 (1992).
- [10] N. J. Zabusky and G. S. Deem, *J. Comput. Phys.* **2**, 126 (1967).
- [11] M. Toda, *J. Phys. Soc. Jpn.* **22**, 431 (1967).
- [12] M. Hénon and C. Heiles, *Astron. J.* **69**, 73 (1964).
- [13] A. N. Kolmogorov, *Dokl. Akad. Nauk SSSR* **98**, 527 (1954).
- [14] V. I. Arnold, *Collected Works: Representations of Functions, Celestial Mechanics and KAM Theory, 1957–1965* (Springer, Berlin, Heidelberg, 2009), p. 267.
- [15] J. Moser, *Matematika* **6**, 51 (1962), <http://mi.mathnet.ru/eng/mat236>.
- [16] C. E. Wayne, *Commun. Math. Phys.* **96**, 311 (1984).
- [17] E. Fermi, P. Pasta, S. Ulam, and M. Tsingou, Studies of the nonlinear problems, Technical Report No. LA-1940, Los Alamos Scientific Lab., N. Mex., 1955.
- [18] C. Danieli, T. Mithun, Y. Kati, D. K. Campbell, and S. Flach, *Phys. Rev. E* **100**, 032217 (2019).
- [19] T. Mithun, C. Danieli, Y. Kati, and S. Flach, *Phys. Rev. Lett.* **122**, 054102 (2019).
- [20] T. Mithun, C. Danieli, M. V. Fistul, B. L. Altshuler, and S. Flach, *Phys. Rev. E* **104**, 014218 (2021).
- [21] T. Goldfriend and J. Kurchan, *Phys. Rev. E* **99**, 022146 (2019).
- [22] S. Ganapa, A. Apte, and A. Dhar, *J. Stat. Phys.* **180**, 1010 (2020).
- [23] M. Baldovin, A. Vulpiani, and G. Gradenigo, *J. Stat. Phys.* **183**, 41 (2021).
- [24] V. I. Oseledets, *Tr. Mosk. Mat. Obs.* **19**, 179 (1968), <http://mi.mathnet.ru/eng/mmo214>.
- [25] A. S. de Wijn, B. Hess, and B. V. Fine, *Phys. Rev. E* **92**, 062929 (2015).
- [26] S. Iubini and A. Politi, *Chaos Solit. Fractals* **147**, 110954 (2021).
- [27] G. Benettin, L. Galgani, A. Giorgilli, and J.-M. Strelcyn, *Meccanica* **15**, 9 (1980).
- [28] I. Vakulchyk, M. V. Fistul, and S. Flach, *Phys. Rev. Lett.* **122**, 040501 (2019).
- [29] I. Vakulchyk, M. V. Fistul, P. Qin, and S. Flach, *Phys. Rev. B* **96**, 144204 (2017).
- [30] M. Malishava, I. Vakulchyk, M. Fistul, and S. Flach, *Phys. Rev. B* **101**, 144201 (2020).
- [31] I. Vakulchyk, M. Fistul, Y. Zolotaryuk, and S. Flach, *Chaos* **28**, 123104 (2018).
- [32] See Supplemental Material at <http://link.aps.org/supplemental/10.1103/PhysRevLett.128.134102> for details on the unitary circuit map, equations of motion in SR and LR networks, and some details on Lyapunov spectrum computation.
- [33] C. Skokos, The Lyapunov characteristic exponents and their computation, in *Dynamics of Small Solar System Bodies and Exoplanets*, edited by J. J. Souchay and R. Dvorak (Springer Berlin Heidelberg, Berlin, Heidelberg, 2010), pp. 63–135.
- [34] M. Mulansky, K. Ahnert, A. Pikovsky, and D. Shepelyansky, *J. Stat. Phys.* **145**, 1256 (2011).
- [35] A. De Wijn, B. Hess, and B. V. Fine, *J. Phys. A* **46**, 254012 (2013).